UNIVERSITY OF AMSTERDAM

UvA-DARE (Digital Academic Repository)

Early stages of drop coalescence

Deblais, Antoine; Xie, Kaili; Lewin-Jones, Peter; Aarts, Dirk; Herrada, Miguel A.; Eggers, Jens; Sprittles, James E.; Bonn, Daniel

DOI
10.1103/PhysRevFluids.10.L042001

Publication date
2025

Document Version
Final published version

Published in
Physical Review Fluids

License
Article 25fa Dutch Copyright Act (https://www.openaccess.nl/en/policies/open-access-in-dutch-copyright-law-taverne-amendment)

Link to publication

Citation for published version (APA):
Deblais, A., Xie, K., Lewin-Jones, P., Aarts, D., Herrada, M. A., Eggers, J., Sprittles, J. E., & Bonn, D. (2025). Early stages of drop coalescence. *Physical Review Fluids*, *10*(4), Article L042001. https://doi.org/10.1103/PhysRevFluids.10.L042001

General rights
It is not permitted to download or to forward/distribute the text or part of it without the consent of the author(s) and/or copyright holder(s), other than for strictly personal, individual use, unless the work is under an open content license (like Creative Commons).

Disclaimer/Complaints regulations
If you believe that digital publication of certain material infringes any of your rights or (privacy) interests, please let the Library know, stating your reasons. In case of a legitimate complaint, the Library will make the material inaccessible and/or remove it from the website. Please Ask the Library: https://uba.uva.nl/en/contact, or a letter to: Library of the University of Amsterdam, Secretariat, P.O. Box 19185, 1000 GD Amsterdam, The Netherlands. You will be contacted as soon as possible.

UvA-DARE is a service provided by the library of the University of Amsterdam (https://dare.uva.nl)

Download date:07 Sept 2026

Letter

Early stages of drop coalescence

Antoine Deblais [1,*] Kaili Xie [1,†] Peter Lewin-Jones [2] Dirk Aarts [3] Miguel A. Herrada [4] Jens Eggers [5] James E. Sprittles [2] and Daniel Bonn [1]

[1]*Van der Waals-Zeeman Institute, Institute of Physics, University of Amsterdam, 1098XH, Amsterdam, The Netherlands*

[2]*Mathematics Institute, University of Warwick, Coventry CV4 7AL, United Kingdom*

[3]*Department of Chemistry, Physical and Theoretical Chemistry Laboratory, University of Oxford, South Parks Road, Oxford OX1 3QZ, United Kingdom*

[4]*Escuela Tecnica Superior de Ingeneria, Universidad de Sevilla, Seville 41092, Spain*

[5]*School of Mathematics, University of Bristol, Fry Building, Woodland Road, Bristol BS8 1UG, United Kingdom*

(Received 1 February 2024; accepted 12 March 2025; published 10 April 2025)

Despite the large body of research on coalescence, firm agreement between experiment, theory, and computation has not been established for the very first moments following the initial contact of two liquid volumes. By combining a range of experimental and computational modeling approaches in two different geometries—namely, drop-drop and drop-bath configurations—we elucidated the influence of the intervening gas and van der Waals forces on coalescence. For the simple liquids considered here, the gas influences both pre- and postcontact regimes, with jump-to-contact being the primary mode of merging. Subsequently, wave-like air pockets are observed and ultimately influence the initial opening dynamics of the neck.

DOI: 10.1103/PhysRevFluids.10.L042001

Introduction. The merging of liquid volumes is important for a plethora of fluid phenomena; for example, drop-drop coalescence dynamics dictate the size of raindrops, efficacy of virus transmission, accuracy of inkjet printing, and efficiency of spraying phenomena [1–5], while drop-surface interactions are key for production of ocean mist, air-sea gas exchange, and airborne salt particles [6,7].

When colliding drops are able to displace the surrounding gas to touch, coalescence is initiated by the formation of a liquid bridge (or neck) between the two drops, which subsequently grows with surface tension, driving the expansion. Depending on the parameter regime, namely, whether it is the viscosity or inertia of the drop that resists the capillary forces, different scalings have been derived for this growth [8–10].

In the conventional hydrodynamic description of coalescence, growth is initially inhibited by the viscosity η of the liquid. The rate of growth is then determined by a balance of capillary and viscous forces, and a simple dimensional analysis then leads directly to a capillary velocity $U_{\rm cap} \approx \gamma/\eta$, with γ surface tension, which gives the rate at which the fluid bridge increases. A more detailed analysis [8] shows there is a logarithmic correction to this, leading to a temporal variation of the bridge radius $R \propto \tau \log \tau$, where $\tau = t\text{-}t_0$ is the time from initial contact t_0.

For the coalescence of water droplets ($\gamma \approx 70$ mN/m and $\eta = 1$ mPa $\cdot$ s), $U_{\rm cap} \approx 70$ m/s. This means that very rapidly the fluid inertia becomes important; the balance between inertial and viscous

*Contact author: a.deblais@uva.nl
†Contact author: k.xie2@uva.nl

 ©2025 American Physical Society

forces is dictated by the local Reynolds number $Re(\tau) = \rho\gamma R^2/R_0\eta^2$, with ρ the density, $R(\tau)$ the radius of the neck, and R_0 the radius of the drop [11]. For millimeter-sized drops of water, $Re \approx 1$ as soon as $R \approx 1\mu$m. Thus, for water, the viscous regime is hard to observe, and the coalescence is, from a practical point of view, completely inertial. The inertial dynamics is then given by

$$R(\tau) = A\left(\frac{\gamma R_0}{\rho}\right)^{1/4}\tau^{1/2}, \tag{1}$$

where the prefactor A covers 1–1.25 from imaging experiment measurement [9,12,13], slightly lower than 1.62 from numerical simulation [14]. For coalescence, simulations and classical theories assume that the initial state consists of two stationary, undeformed spherical drops joined by a very small liquid bridge, with the Laplace pressure for a vanishing contact radius approaching infinity. This poses the question of how these drops actually come into contact and displace the intervening gas.

Experimentally, this is a very difficult question, as direct imaging is evidently limited by both the optical resolution and the rate at which images can be acquired [9,12]. In addition, focusing on the plane of the coalescing drops and "seeing into" its cusp-like region may lead to spurious exponents for the dynamics, as shown in Ref. [15]. To overcome these issues, Paulsen *et al.* [11,16] deployed an electrical method to infer the radius of the bridge in the early stages and proposed a new initial regime in which inertia, capillarity, and viscosity are all important. However, simulations of the full Navier-Stokes system [17,18] show no evidence for this regime, so the links between experiment and theory remain unclear.

In this work, we study the initial stages of inertial drop coalescence at extremely short times ($\approx$0.1 μs) and small length scales ($\approx$2 μm) in two configurations, drop-drop and drop-bath, elucidating the role of initial contact and air drainage in the dynamics of neck opening. In the drop-drop configuration, we show that, with good control of initial conditions in the electrical setup, the dynamics of the neck opening follows the expected inertial scaling without deviation, suggesting that previous experimental discrepancies were due to initial interface deformation caused by undesired charges. In the drop-bath configuration, we develop a new imaging setup that enables us to directly visualize the evolution of the air-liquid interface over time. We show for the first time that the rupture of an air film during the merging of a drop with a bulk liquid occurs with a jump to contact, generating capillary waves at the liquid surface ahead of an entrapped air pocket. This consequently affects the inertial opening dynamics at the very first moments after coalescence. In both cases, our experimental observations agree well with direct simulations that incorporate both liquid and gas phases without assuming an initially spherical shape. Instead, we precompute the initial conditions based on the approach problem, allowing us to accurately model the two different configurations.

Drop-drop. We use an electrical technique similar to those described in Refs. [11,16,19,20] to measure the coalescence between two drops. The experiments consist of two electrodes facing each other, each holding a liquid droplet. The upper electrode is translated downward using a speed-controlled translation stage. We used salt water (NaCl) with high conductivity (30 mS/cm, see Supplemental Table 1). Our electrical setup allows us to achieve micron spatial and $\sim$100 nanosecond temporal resolution. By minimizing applied voltage and undesired surface charges before coalescence, we ensure the droplet remains spherical rather than conical, as the initial shape strongly influences neck-opening dynamics [15,21] (see Supplemental Material Part Ic in [24], including Refs. [15,19,20,25,31–34]).

In Fig. 1(a), we plot the measured conductivity as a function of time. The shape of the liquid bridge is computed from a simulation, allowing us to calculate the radius of the neck over time. We use a numerical scheme based on a volume-of-fluid method provided by the Basilisk software [22], which uses QUADTREES [23] to allow efficient adaptive grid refinement of the interface close to the coalescence region (Supplemental Material [24]). The measured resistance of the liquid bridge data is well described by the simulations at an early stage of the coalescence point.

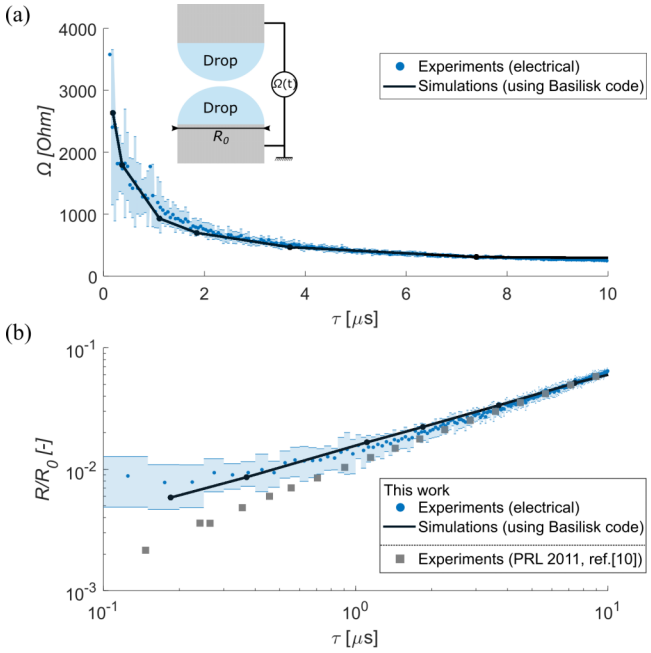

FIG. 1. (a) Electrical resistance Ω of a low-viscous saline capillary bridge ($\eta = 1.8$ mPa s) between two electrodes ($R_0 = 1$ mm) as a function of time. The upper electrode moves at a very low constant downward speed, initiating coalescence; the electrical resistance is obtained from the complex impedance of the circuit, following the method detailed in Ref. [16]. (b) From the electrical resistance shown in (a), the opening dynamics of the neck can be calculated by Eq. 2. Data from Ref. [11] are also plotted for comparison (viscosity $\eta = 1.9$ mPa · s). Dots represent averaged values for three different experiments, while the shaded area corresponds to standard deviations.

Figure 1(b) shows the minimum neck radius R/R_0 as a function of time after coalescence as follows from the electrical measurements: the neck diameter is obtained using relation [16],

$$R = 2\left[3.62\sigma\left(\Omega - \frac{1}{\pi R_0 \sigma}\right)\right]^{-1}, \tag{2}$$

with Ω the electrical resistance and σ the conductivity of the fluid, which we also confirm from our simulation (Fig. S3 in Supplemental Material [24]). The dynamics follow the form $R(\tau) \propto \tau^{\alpha}$, for which we recover $\alpha = 0.5$ for the inertial case. We attribute the different slope observed by Paulsen *et al.* [11] at early times to the initial deformation of the interface due to the presence of charges and the use of a liquid with lower conductivity. To validate this hypothesis, we conduct experiments in which we preliminarily charged the drops and compare the dynamics with drops that remained uncharged. In the presence of charges, side-view images show conical-like deformation (Fig. S4 in Supplemental Material) of the interface and cause immediate deviations from the $t^{1/2}$ inertial scaling to $\sim t^{2/3}$ [15]. However, in the absence of optical imaging at these time scales and spatial scales, we have no information about how the initial contact occurs or the subsequent shape of the interface. These results nonetheless suggest that the details of how the drops are brought into contact can affect the opening dynamics, which will take on its importance later.

To access this initial precontact approach stage, we deploy bespoke finite-element simulations for the drop dynamics, which include the influence of the gas, with corrections due to kinetic effects for microscale gas films, alongside van der Waals forces; see Refs. [25,26] for details of the computational framework. In Fig. 2, we see that, for the slow approach speeds considered in our

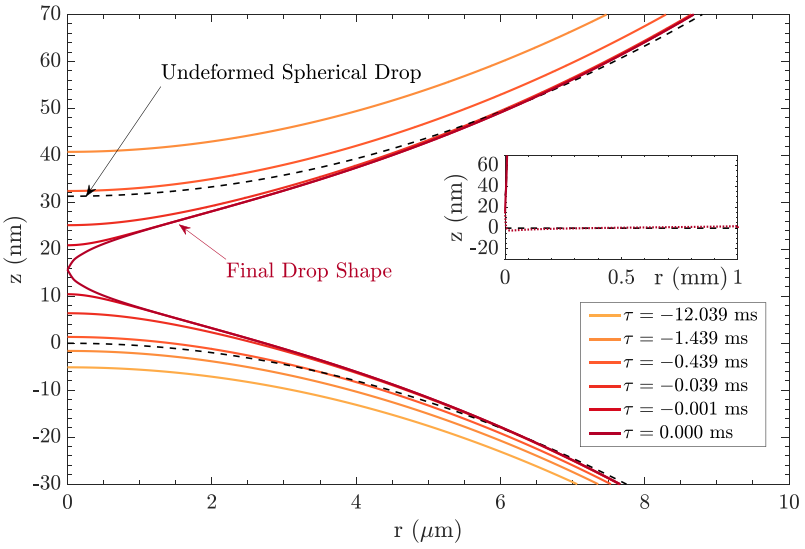

FIG. 2. Computed interface profiles of the final stages of a drop moving toward another drop at 5 μm/s, just before first contact at $\tau = 0$. The inset shows the position of the upper drop and the vertical displacement of the lower drop from its undeformed spherical shape at $\tau = 0$ – clearly, this is localized near $r = 0$. The earliest timestep shown is when the flattening of the lower drop due to the gas film is maximal.

experiments, the deformation of the drops caused by gas lubrication is relatively small so that the interfaces meet at $r = 0$, that is, no bubble is entrapped. Notably, the van der Waals force causes a jump to contact when the separation of the drops is ≈30 nm over a timescale of ∼0.1 ms. Separations of tens of nanometers are consistent with the literature [27–30] and were previously observed for atomic force microscopy (AFM) tips that connect to a fluid surface.

Drop-bath. To access the initial stages of coalescence optically, we turn to the drop-bath configuration and use a novel approach by viewing the event from "underneath" to overcome spurious effects due to side imaging [15,31], where it is not possible to measure small contact radii (less than 20 μm). The setup consists of a drop on a needle to which liquid is supplied slowly by a syringe pump. This drop is facing a bath of the same liquid (Supplemental Fig. S7, [24]). Our needle tip is millimetric, and a drop is slowly grown at its tip until it coalesces with the bulk (growing velocity $\leqslant 20$ μm/s, to minimize the effect of air drainage between the droplet and the bulk surface). The viscosity, density, and surface tension are given in Supplementary Table S1 [24]. All experiments were performed at room temperature (22 ± 1 °C) and atmospheric pressure.

The growth of the neck bridging the droplet with its bulk is recorded from below through the bath using an inverted microscope (Zeiss Axiovert A1) at a frame rate of up to 1 000 000 fps using a high-speed camera (Phantom TMX 7510), allowing us to reach a spatial resolution of typically 0.9 μm/pix. The minimum radius of the neck R is followed in time by an image analysis routine (Fig. 3).

Figure 3(a) shows a sequence of the neck opening during coalescence for the droplet-bulk geometry, exhibiting two key features. It is immediately clear that (i) there is an abrupt change in intensity corresponding to the coalesced bridge radius, and (ii) there are concentric rings ahead of the bridge, as seen in Fig. 3(b), which appear to be the signature of interfacial waves refracting passing light. This is confirmed by examining the interface profile obtained from the Basilisk simulations at a specific time ($\tau = 64$ μs), shown in Fig. 3(c), where waves are observed ahead of an air pocket. This combination of inertial coalescence driving wave formation and gas lubrication preventing the pinching of toroidal bubbles has been previously described theoretically and in simulations [14,17],

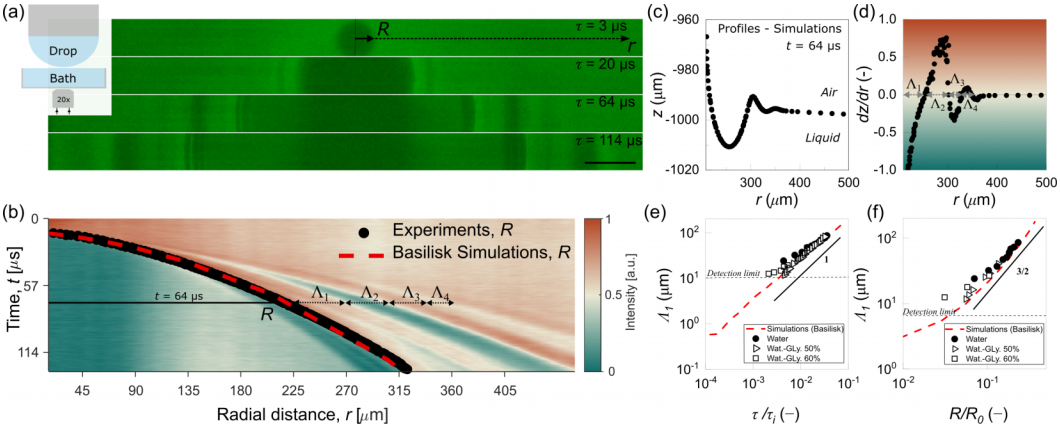

FIG. 3. (a) Image sequences captured from the bottom view using a fast camera. The photographs depict the very early stages of bath interface coalescence, where the droplet (water, $R_0 = 0.9\,\text{mm}$) contacts the lower bath. (b) Corresponding spatiotemporal averaged intensity of (a). Black dot points indicate the tracked minimum neck diameter R, and the dashed red line represents the Basilisk simulation for the same droplet radius R_0 as in (a). As the minimum neck diameter increases, capillary waves are excited ahead of the front, as shown by the change in intensity. (c) Profiles of the interface extracted from the simulation at $\tau = 64$ μs after coalescence (left), and its corresponding first derivative (right). We define the lengths Λ_i for which the local derivative is positive or negative. These lengths correspond to the change in intensity observed in (b) as a result of the refraction of light at the bath interface. (e),(f) The first length Λ_1 corresponding to the air pocket size in (c) as a function of the rescaled time (with the inertial time $\tau_i = \sqrt{\rho R_0^3/\gamma}$) and the rescaled minimum neck radius.

and is also predicted for viscous coalescence [8], but direct and strong experimental evidence for it was lacking until now.

To further confirm this hypothesis, in Fig. 3(d) we plot the spatial deformation (dz/dr), obtained from the simulations to define domains Λ_i, where the interface undergoes pronounced changes. In Fig. 3(b), we show that this aligns with experimentally observed intensity variations. The characteristic size of the first domain Λ_1, which corresponds to the air pocket size shown in Fig. 3(c), is shown in Figs. 3(e) and 3(f) as a function of time and neck radius, respectively. Simulations and experimental results again show good agreement and demonstrate that the air pocket grows linearly in time [Fig. 4(e)] and as $R^{3/2}$, as predicted by theory [8], regardless of the different viscosities of fluids (1 mPa · s to 11.5 mPa · s) we tested in our experiments.

As shown in Fig. 4, for the late stage of coalescence, the inertial-capillary regime of drop-drop coalescence is recovered with $R(\tau) \sim \tau^{1/2}$. In the early stage, a different regime is observed for all fluids, with a radius smaller than what would be expected from the inertial-capillary regime; Something else slows down the coalescence. For this earlier regime, all the curves collapse when scaled with the inertial time: There is no effect of viscosity. We therefore look into the dynamics of the air film.

In our experiments, we observe interference fringes between the two surfaces in the last frames before coalescence (see Supplemental Fig. S8), which suggests the presence of a thin air film that acts as a lubricant between the two approaching surfaces. This air film continually thins, and if it becomes thin enough, the two surfaces jump into contact. This behavior is also confirmed by finite-element simulations in Fig. 5, showing the final moments of the approach of a drop toward a liquid bath before coalescence. The gas is modeled using a lubrication equation and incorporates the van der Waals-driven disjoining pressure that causes the jump to contact, as well as gas kinetic factors that account for microscale gas films, as described in Ref. [25]. Figure 5 shows that the bath is pushed down vertically ∼30 nm over the radial extent of the drop ∼mm before the drop jumps

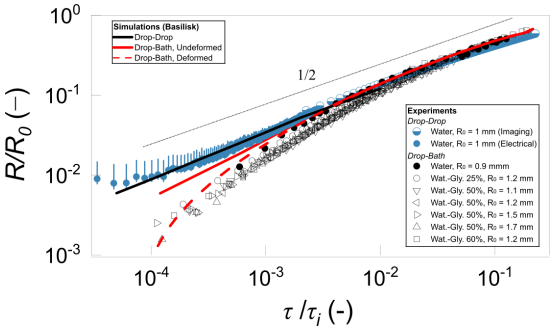

FIG. 4. Rescaled radius (with $R_0 = [0.9; 1.73]$ mm) versus rescaled time for the different liquids investigated in the drop-bath configurations and plotted together with the drop-drop configuration (Fig. 1) for direct comparison. Lines show the results obtained from simulations (Basilisk) and symbols from experiments (imaging and electrical).

to contact, over a radial extent ∼3 µm in ∼0.1 ms, similar to the mechanism seen in the drop-drop case but with a vertical shift.

All this suggests that the initial deformation of the interfaces due to the presence of the air film can change the initial opening dynamics of the liquid bridge, and this effect is more important for the drop-bath than for the drop-drop case, because of their different geometries. To see whether we can reproduce the dynamics of the radius, Basilisk simulations (dashed red line) of the droplet-bulk coalescence for water succeed in qualitatively describing the deviation from the $t^{1/2}$ law; we use an initial neck diameter of 2.7 µm, which is the smallest size feasible in these simulations. To achieve this agreement, the time axis in the simulation was set to match the experiments [Fig. 3(b)]; adjusting the time is rather standard and amounts to fixing the coalescence time t_0. If we use the final profiles

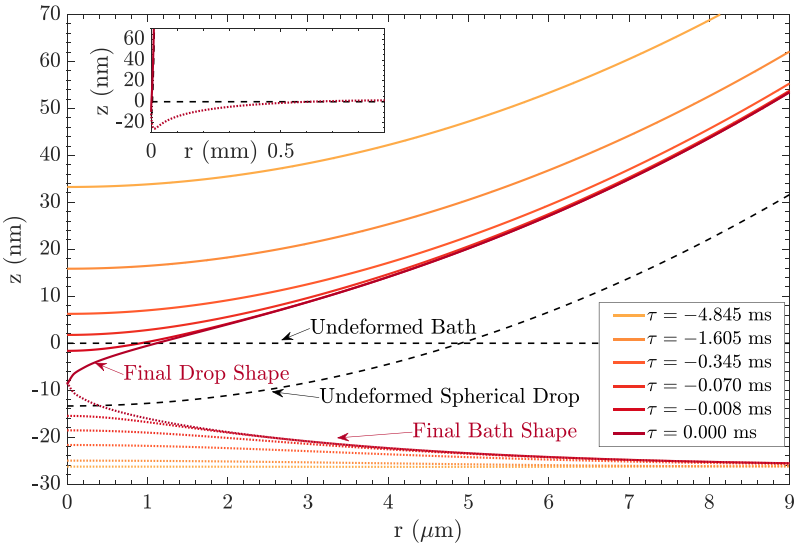

FIG. 5. Same graph as in Fig. 2, but here we computed the interface profiles of the final stages of a drop moving toward a liquid bath before first contact at $\tau = 0$ (approach speed is 5 µm/s). The inset shows the extent of the deformation of the drop and bath at the moment of contact, highlighting differences with the drop-drop case. The earliest timestep shown is when the deformation of the bath due to the gas film is maximal.

from the finite-element calculation as a starting point, we get a much better agreement (dashed red line, showing again that the initial deformation is important. However, to obtain this agreement, in both the deformed and undeformed cases, we had to adjust the initial minimum neck diameter R by 50 μm to align the experiments with the simulations (see the comparison in Supplemental Fig. S9). It is perhaps unsurprising that a small spatial shift is required to account for the missed dynamics; in fact, it is rather remarkable that this shift alone is sufficient to achieve good agreement with experiments at later stages. The physical reason behind this shift presents an interesting open question for future work.

Our findings open several exciting avenues for future research. The ultrafast imaging techniques we deployed, combined with high-precision interferometry, could provide deeper insights into the initial contact dynamics and the evolution of the air film. Additionally, finite-element simulations that bridge the pre- and postcontact regimes would offer a more comprehensive understanding of the complex interplay between inertial, capillary, and viscous forces during coalescence. Furthermore, our work has potential applications in microfluidics, inkjet printing, and emulsion stabilization, where precise control over droplet coalescence is crucial. Exploring these applications could lead to innovative advancements in controlling droplet behavior in flows and ensuring film stability across various technologies.

Acknowledgments. We are very grateful to the technology center of the University of Amsterdam for technical assistance with the electrical setup. D.B. thanks Jacco Snoeijer for very helpful discussions about the artifacts induced by side imaging. J.E.S. acknowledges the support of the EPSRC under Grants No. EP/W031426/1, No. EP/S022848/1, No. EP/S029966/1, No. EP/P031684/1, and No. EP/V012002/1. P.L.-J. is supported by a studentship within the UK EPSRC-supported Centre for Doctoral Training in the Modeling of Heterogeneous Systems (HetSys), EP/S022848/1.

[1] D. Lohse, Fundamental fluid dynamics challenges in inkjet printing, Annu. Rev. Fluid Mech. **54**, 349 (2022).

[2] A. Glasser, E. Cloutet, G. Hadziioannou, and H. Kellay, Tuning the rheology of conducting polymer inks for various deposition processes, Chem. Mater. **31**, 6936 (2019).

[3] M. Liu, J. Wang, M. He, L. Wang, F. Li, L. Jiang, and Y. Song, Inkjet printing controllable footprint lines by regulating the dynamic wettability of coalescing ink droplets, ACS Appl. Mater. Interfaces **6**, 13344 (2014).

[4] G. A. Somsen, C. van Rijn, S. Kooij, R. A. Bem, and D. Bonn, Small droplet aerosols in poorly ventilated spaces and SARS-CoV-2 transmission, Lancet Respir. Med. **8**, 658 (2020).

[5] S. Kooij, C. van Rijn, N. Ribe, and D. Bonn, Self-charging of sprays, Sci. Rep. **12**, 19296 (2022).

[6] R. Wanninkhof, W. E. Asher, D. T. Ho, C. Sweeney, and W. R. McGillis, Advances in quantifying air-sea gas exchange and environmental forcing, Annu. Rev. Marine Sci. **1**, 213 (2009).

[7] F. Raes, R. Van Dingenen, E. Vignati, J. Wilson, J.-P. Putaud, J. H. Seinfeld, and P. Adams, Formation and cycling of aerosols in the global troposphere, Atmospheric Environ. **34**, 4215 (2000).

[8] J. Eggers, J. R. Lister, and H. A. Stone, Coalescence of liquid drops, J. Fluid Mech. **401**, 293 (1999).

[9] D. G. A. L. Aarts, H. N. W. Lekkerkerker, H. Guo, G. H. Wegdam, and D. Bonn, Hydrodynamics of droplet coalescence, Phys. Rev. Lett. **95**, 164503 (2005).

[10] J. Eggers, J. E. Sprittles, and J. H. Snoeijer, Coalescence Dynamics, Annu. Rev. Fluid Mech. **57**, 61 (2025).

[11] J. D. Paulsen, J. C. Burton, and S. R. Nagel, Viscous to inertial crossover in liquid drop coalescence, Phys. Rev. Lett. **106**, 114501 (2011).

[12] M. Wu, T. Cubaud, and C.-M. Ho, Scaling law in liquid drop coalescence driven by surface tension, Phys. Fluids **16**, L51 (2004).

[13] S. T. Thoroddsen, K. Takehara, and T. G. Etoh, The coalescence speed of a pendent and a sessile drop, J. Fluid Mech. **527**, 85 (2005).

[14] L. Duchemin, J. Eggers, and C. Josserand, Inviscid coalescence of drops, J. Fluid Mech. **487**, 167 (2003).
[15] A. Eddi, K. G. Winkels, and J. H. Snoeijer, Influence of droplet geometry on the coalescence of low viscosity drops, Phys. Rev. Lett. **111**, 144502 (2013).
[16] J. D. Paulsen, Approach and coalescence of liquid drops in air, Phys. Rev. E **88**, 063010 (2013).
[17] J. E. Sprittles and Y. D. Shikhmurzaev, A parametric study of the coalescence of liquid drops in a viscous gas, J. Fluid Mech. **753**, 279 (2014).
[18] C. R. Anthony, M. T. Harris, and O. A. Basaran, Initial regime of drop coalescence, Phys. Rev. Fluids **5**, 033608 (2020).
[19] S. C. Case, Coalescence of low-viscosity fluids in air, Phys. Rev. E **79**, 026307 (2009).
[20] J. D. Paulsen, J. C. Burton, S. R. Nagel, S. Appathurai, M. T. Harris, and O. A. Basaran, The inexorable resistance of inertia determines the initial regime of drop coalescence, Proc. Natl. Acad. Sci. USA **109**, 6857 (2012).
[21] J. C. Bird, W. D. Ristenpart, A. Belmonte, and H. A. Stone, Critical angle for electrically driven coalescence of two conical droplets, Phys. Rev. Lett. **103**, 164502 (2009).
[22] http://basilisk.fr/.
[23] S. Popinet, Quadtree-adaptive tsunami modelling, Ocean Dynamics **61**, 1261 (2011).
[24] See Supplemental Material at http://link.aps.org/supplemental/10.1103/PhysRevFluids.10.L042001 for more details on the experimental methods, set-up, and simulations, which includes Refs. [15,19,20,25,31–34].
[25] J. E. Sprittles, Gas microfilms in droplet dynamics: When do drops bounce? Annu. Rev. Fluid Mech. **56**, 91 (2024).
[26] P. Lewin-Jones, D. A. Lockerby, and J. E. Sprittles, Collision of liquid drops: Bounce or merge? J. Fluid Mech. **995**, A1 (2024).
[27] R. Ledesma-Alonso, P. Tordjeman, and D. Legendre, Multiscale deformation of a liquid surface in interaction with a nanoprobe, Phys. Rev. E **85**, 061602 (2012).
[28] R. Ledesma-Alonso, D. Legendre, and P. Tordjeman, Nanoscale deformation of a liquid surface, Phys. Rev. Lett. **108**, 106104 (2012).
[29] V. Chireux, M. Protat, F. Risso, T. Ondarçuhu, and P. Tordjeman, Jump-to-contact instability: The nanoscale mechanism of droplet coalescence in air, Phys. Rev. Fluids **3**, 102001(R) (2018).
[30] V. Chireux, P. Tordjeman, and F. Risso, Bridge expansion after coalescence of two droplets in air: Inertial regime, Phys. Fluids **33**, 062112 (2021).
[31] K. G. Winkels, J. H. Weijs, A. Eddi, and J. H. Snoeijer, Initial spreading of low-viscosity drops on partially wetting surfaces, Phys. Rev. E **85**, 055301(R) (2012).
[32] A. Deblais, M. A. Herrada, I. Hauner, K. P. Velikov, T. van Roon, H. Kellay, J. Eggers, and D. Bonn, Viscous effects on inertial drop formation, Phys. Rev. Lett. **121**, 254501 (2018).
[33] M. Heil, A. Hazel, and M. Puneet, Oomph-lib, https://github.com/oomph-lib/oomph-lib (2022).
[34] K. Takamura, H. Fischer, and N. R. Morrow, Physical properties of aqueous glycerol solutions, J. Pet. Sci. Eng. **98-99**, 50 (2012).